

Discovery Potential of Future Electron-Positron Colliders for a 95 GeV Scalar

Pramod Sharma^{a,b}, Anza-Tshilidzi Mulaudzi^{a,c}, Karabo Mosala^{a,c}, Thuso Mathaha^{a,c}, Mukesh Kumar^a, Bruce Mellado^{a,c}, Andreas Crivellin^{d,e}, Maxim Titov^f, Manqi Ruan^g, Yaquan Fang^h

^a*School of Physics and Institute for Collider Particle Physics, University of the Witwatersrand, Johannesburg, Wits 2050, South Africa.*

^b*Indian Institute of Science Education and Research, Knowledge City, Sector 81, S. A. S. Nagar, Manauli PO 140306, Punjab, India.*

^c*iThemba LABS, National Research Foundation, PO Box 722, Somerset West 7129, South Africa*

^d*Paul Scherrer Institut, CH-5232 Villigen PSI, Switzerland*

^e*Physik-Institut, Universität Zürich, Winterthurerstrasse 190, CH-8057 Zürich, Switzerland*

^f*Commissariat à l'Énergie Atomique et Énergies Alternatives (CEA) Saclay Direction de la Recherche Fondamentale (DRF) Institute of Research into the Fundamental Laws of Universe (IRFU) 91191 Gif sur Yvette Cedex, France*

^g*Institute of High Energy Physics, Chinese Academy of Sciences, Beijing, 100049, China*

^h*University of Chinese Academy of Sciences, Beijing, 100049, China*

arXiv:2407.16806v3 [hep-ph] 21 Nov 2024

Abstract

The Large Electron Positron collider observed an indication for a new Higgs boson with a mass around 95 GeV-100 GeV in the process $e^+e^- \rightarrow Z^* \rightarrow ZS$ with $S \rightarrow b\bar{b}$. The interest in this excess re-emerged with the di-photon signature at ≈ 95 GeV at the Large Hadron Collider. In fact, a combined global significance of 3.4σ is obtained once WW and $\tau\tau$ signals are included in addition. In this article, we perform a feasibility study for discovering such a new scalar S at future electron-positron colliders using the recoil-mass method applied to $e^+e^- \rightarrow ZS$ with $Z \rightarrow \mu^+\mu^-$ and $S \rightarrow b\bar{b}$. For this, we employ a Deep Neural Network to enhance the separation between the Standard Model background and the signal, reducing the required integrated luminosity necessary for discovery by a factor of two to three. As a result, an $SU(2)_L$ singlet Higgs with a mass of ≈ 95 GeV can be observed with more than 5σ significance at a 250 GeV centre-of-mass energy collider with 5 ab^{-1} integrated luminosity if it has a mixing angle of at least 0.1 with the Standard Model Higgs, which means that a discovery can be achieved within the whole 95% confidence-level region preferred by Large Electron Positron excess. Furthermore, including more decay channels such as $S \rightarrow \tau\tau$ and $Z \rightarrow e^+e^-$ further enhances the discovery potential of future e^+e^- accelerators, like CEPC, CLIC, FCC-ee and ILC.

Keywords: Higgs, CEPC, Future e^+e^- -collider, Beyond the Standard Model, Machine Learning

1. Introduction

The discovery of the Higgs boson (h) [1–4] at the Large Hadron Collider (LHC) at CERN was of momentous importance for particle physics [5, 6]. It is the only fundamental scalar particle (to our current knowledge) and triggers the mechanism of spontaneous symmetry breaking of the weak interactions in the Standard Model (SM) [7–9]. Therefore, the particle content of the SM is finally completely observed, about six decades after its inception, and the discovery of a new (fundamental) particle would prove the existence of beyond-the-SM physics.

Because no symmetry principle or consistency requirement prohibits the extension of the SM by additional Higgs bosons, the minimality of the SM scalar sector is an outstanding issue that requires further investigation, particularly experimental searches. In this context, it is interesting that the Large Electron-Positron

(LEP) Collider at CERN reported in 2003 a mild excess with a local significance of 2.3σ in the search for a new Higgs boson (S) in the range of 95 GeV-100 GeV using the process $e^+e^- \rightarrow ZS$ with $S \rightarrow b\bar{b}$ [10], called Higgsstrahlung. However, due to the start of LHC construction further experimental scrutiny of this excess at LEP was not possible anymore¹ and the $b\bar{b}$ channel is difficult to test at this mass range at the LHC due to the large QCD background.

Renewed interest in this excess emerged in 2018 when the CMS experiment released an analysis with an excess at ≈ 95 GeV in the di-photon invariant mass spectrum based on run-1 and partial run-2 data [12]. This result was later updated to include the full run-2 data, resulting in local (global) significance of 2.9σ (1.3σ) [13]. Furthermore, ATLAS reported a smaller but consistent excess of 1.7σ (locally) at the same mass [14] in di-photon final states and a 2.8σ indication in the search for additional Higgs bosons in $\tau^+\tau^-$ was found by CMS [15].² In addition, an $\approx 2.5\sigma$ excess (at ≈ 95 GeV) has been found in

Email addresses: pramodsharma.iiser@gmail.com (Pramod Sharma), anza-tshilidzi.mulaudzi@cern.ch (Anza-Tshilidzi Mulaudzi), karabo.mosala@cern.ch (Karabo Mosala), thuso.mathaha@cern.ch (Thuso Mathaha), mukesh.kumar@cern.ch (Mukesh Kumar), bmellado@mail.cern.ch (Bruce Mellado), andreas.crivellin@cern.ch (Andreas Crivellin), maksym.titov@cern.ch (Maxim Titov), manqi.ruan@ihep.ac.cn (Manqi Ruan), yaquan.fang@cern.ch (Yaquan Fang)

¹The findings in Ref. [11] suggest that the observed excess around 95 GeV for a Higgs-like signal at LEP is most likely a statistical fluctuation of the background.

²Note that even though there is no dedicated ATLAS search in this channel, the side-band in the measurement of the Higgs boson cross-section in $\tau^+\tau^-$ final state [16] shows no excess, resulting in a reduction of the significance

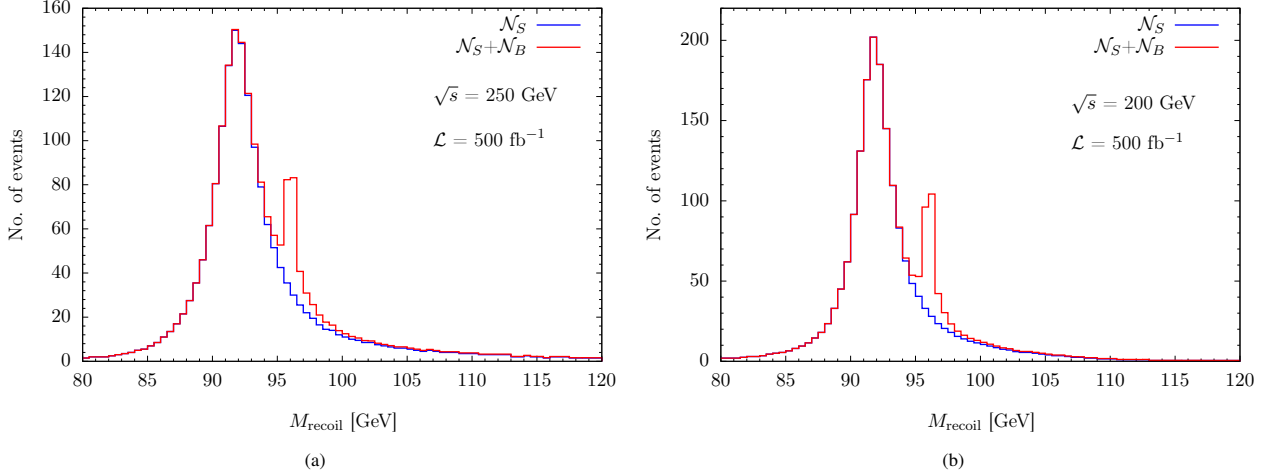


Figure 1: Recoil-mass distribution of the simulated SM background (N_B) and the simulated signal plus background ($N_S + N_B$) for $m_S = 95.5$ GeV for (a) $\sqrt{s} = 250$ GeV and (b) $\sqrt{s} = 200$ GeV at $\mathcal{L} = 500\text{fb}^{-1}$.

the $W^+W^- \rightarrow \ell^+\ell^-\nu\nu$, $\ell = e, \mu$ channel [17] by recasting the corresponding ATLAS and CMS SM Higgs analyses [18, 19]. Upon combining these channels, the global significance of the excesses at ≈ 95 GeV is 3.4σ [20].³ The ATLAS and CMS collaborations [21, 22] conducted a search for a scalar boson in the mass range of 60 to 110 GeV in the diphoton final state, with no significant excess observed.

Due to these indications for the existence of a new Higgs boson at 95 GeV, many extensions of the SM accommodating such an excess have been proposed [23–65]. Interestingly, since a light SM-like Higgs with a mass around 95 GeV naturally decays dominantly to bottom quarks, such a boson is a prime candidate to explain the presence of b -quarks in the LHC multi-lepton anomalies [66–70] (for recent reviews see Refs. [71, 72]). In particular, differential top-quark cross sections favour such a model with at least 5.8σ significance over the SM hypothesis [57] and in a UV complete model also the resonant $t\bar{t}$ excess of CMS [73] can be explained [58]. However, distinguishing between different modes at the LHC is not always feasible due to the large background and the limited detector resolution for bottom quarks such that reaching the discovery threshold of 5σ is difficult, assuming that the currently preferred signal strength corresponds to the true value.

Therefore, we examine in this article the discovery prospects for a 95 GeV Higgs boson at future e^+e^- accelerators, such as the Circular Electron-Positron Collider (CEPC) [74, 75], the Compact Linear Collider (CLIC) [76], the Future Circular Collider (FCC-ee) [77, 78] and the International Linear Collider (ILC) [79, 80]. At these colliders, a scalar S with a $m_S \approx 95$ GeV can be produced via $e^+e^- \rightarrow Z^* \rightarrow ZS$ and the decay modes $Z \rightarrow \mu^+\mu^-$ and $S \rightarrow b\bar{b}$ result in the most prominent signature. For our analysis, we consider the background process

$e^+e^- \rightarrow Zb\bar{b}$ where $Z \rightarrow \mu^+\mu^-$ and use a deep neural network to enhance the discrimination of the signal (Higgs-strahlung process) from the background by employing the recoil mass method.

2. Analysis and Results

To assess the physics potential of future e^+e^- colliders such as CEPC, FCC-ee, CLIC, and ILC, a comprehensive list of Higgs benchmark studies was provided in Ref. [81]. They utilized Geant4 [82, 83] simulations for the proposed detectors [84, 85], based on the concepts developed for the ILC [86]. In these studies, the simulations accounted for all relevant SM background processes, as well as for pile-up from $\gamma\gamma \rightarrow$ hadrons, including the beam spectrum and initial state radiation.

Higgs-strahlung, i.e. $e^+e^- \rightarrow Z^*S$, is the dominant Higgs boson production mechanism at center-of-mass (c.o.m.) energies of $220\text{ GeV} \lesssim \sqrt{s} \lesssim 350\text{ GeV}$ while Higgs production through WW and ZZ fusion is subleading for SM-like Higgses [87]. It allows for a precise measurement of the SZZ coupling in a model-independent approach, the ‘ κ -framework’ where the SZZ coupling is parametrized by a factor κ_Z such that $\kappa_Z = 1$ for the SM Higgs. A measurement of κ_Z can be performed at lepton colliders using the Z -boson recoil mass, specifically for events where $Z \rightarrow \mu^+\mu^-$. Since muons can be well identified, along with their momenta measured in the detector, Higgs-strahlung events can be identified using the recoil-mass method by tagging muon pairs [87]. The recoil mass is defined as:

$$M_{\text{recoil}} = \sqrt{s + M_{\mu^+\mu^-}^2 - 2(E_{\mu^+} + E_{\mu^-})\sqrt{s}}, \quad (1)$$

such that reconstructing the Higgs boson mass is not required. Here, $M_{\mu^+\mu^-}$ is the invariant mass of the muon pair, and E_{μ^+} and E_{μ^-} are the energies of the positively and negatively charged muons, respectively. As shown in Figure 1, the M_{recoil} distribution exhibits a sharper peak around m_S at $\sqrt{s} = 200$ GeV compared to $\sqrt{s} = 250$ GeV. This improvement can be attributed

by approximately a factor $\sqrt{2}$. Furthermore, also CMS finds no excess in b -associated production of a Higgs in the di-tau channel at around 95 GeV.

³In the combination of Ref. [20] the LEP excess was used to narrow down the mass range to reduce the look-elsewhere effect but not including directly in the calculation of the significance.

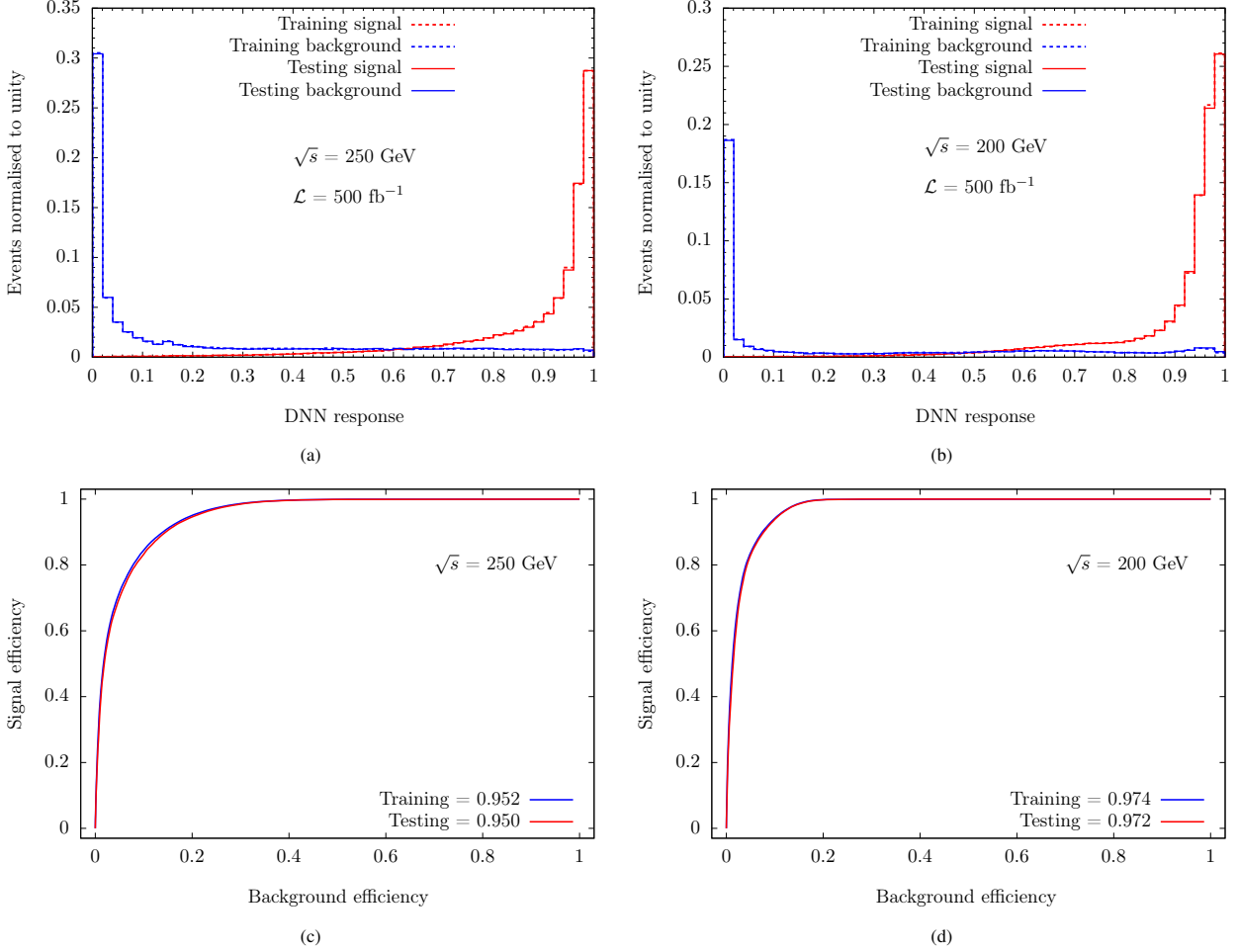


Figure 2: Fraction of events falling to the DNN bins for a center-of-mass energy of (a) $\sqrt{s} = 250$ GeV, and (b) $\sqrt{s} = 200$ GeV, along with the respective ROC curves, (c) and (d).

to the dependence of M_{recoil} on $M_{\mu^+\mu^-}$ reconstruction, which performs better at lower c.o.m. energies due to reduced boost effects.

2.1. Signal and background discrimination

For the signal of a new Higgs boson S , we simulated the Higgs-strahlung process $e^+e^- \rightarrow Z^*S$ with $Z \rightarrow \mu^+\mu^-$ and $S \rightarrow b\bar{b}$, as well as the background process $e^+e^- \rightarrow Zb\bar{b}$ with $Z \rightarrow \mu^+\mu^-$, at a future electron-positron collider by generating one million events. These simulations were conducted for $m_S = 95.5$ GeV scalar at center of mass (c.o.m.) energies of $\sqrt{s} = 200$ GeV and $\sqrt{s} = 250$ GeV, using the Monte Carlo event generator MadGraph5 [88]. The BSM signal is assumed to be 10% of the production cross-section of a (hypothetical) SM-like Higgs-boson with $m_S = 95.5$ GeV in the following (if not defined otherwise). The generation-level cuts were applied to the transverse momentum ($p_{T\mu}$), pseudo-rapidity (η_μ) of the muons, and the angular distance between the muons ($\Delta R_{\mu^+\mu^-}$), as $p_{T\mu} > 10$ GeV, $|\eta_\mu| < 2.5$, and $\Delta R_{\mu^+\mu^-} > 0.4$, respectively.

Following this, we performed the showering, fragmentation, and hadronization of the events with Pythia8 [89] and incorporated the detector simulation via Delphes [90] based on the

proposed CEPC detector design [91, 92]. Jets are clustered by FastJet [93] with the anti- k_T algorithm [94] using the distance parameter $R = 0.4$ and using a dynamic scale both for the factorization and the renormalization.

To optimize the ratio of signal over background, we require exactly two muons and two b -tagged jets and apply minimal cuts on the energy of the b -tagged jets and muon of $E_{b,\mu} > 5$ GeV. Additionally, we use Equation 1 to compute the recoil mass for both signal and background shown in Figure 1a (Figure 1b), and impose $M_{\text{recoil}} < 120$ GeV and $M_{b\bar{b}} < 100$ GeV cuts on signal and background events for $\sqrt{s} = 250$ (200) GeV. Out of the one-million unweighted events generated in MadGraph5, 330,569 (307,988) signal events and 206,201 (289,502) background events survive the cuts for $\sqrt{s} = 250$ GeV (200 GeV). These optimization cuts enhance the signal-to-background ratio, defined over the whole M_{recoil} range, increasing the significance from 2.4σ to 3.4σ at $\mathcal{L} = 500 \text{ fb}^{-1}$ for $\sqrt{s} = 250$ GeV for $\kappa_Z^2 = 0.1$ (before using the DNN) as summarized in Table 1.

Machine Learning model: For performing the machine learning (ML) analysis to improve on the discrimination between signal and background, we use a Deep Neural Network (DNN) which is structured as a Sequential Neural Network. It has a lin-

Kinematic cuts	\mathcal{N}_S	\mathcal{N}_B	significance
At least 2 b -tagged jets and 2 muons	188 (219)	2926 (1876)	2.4σ (3.8σ)
$E_{b,\mu} > 5$ GeV	188 (219)	2924 (1874)	2.4σ (3.8σ)
$M_{b\bar{b}} < 100$ GeV	187 (217)	2223 (1864)	2.9σ (3.8σ)
$M_{\text{recoil}} < 120$ GeV	184 (216)	1732 (1851)	3.4σ (3.8σ)
93.5 GeV $< M_{\text{recoil}} < 97.5$ GeV (before DNN)	150 (193)	288 (274)	8.4σ (11.1σ)
93.5 GeV $< M_{\text{recoil}} < 97.5$ GeV (after DNN)	54 (71)	14 (14)	14.5σ (18.9σ)

Table 1: Cut-flow table showing the number of events for the signal (\mathcal{N}_S) and background (\mathcal{N}_B), along with the significance for the signal (as defined in Equation 5), after each kinematic cut for $\sqrt{s} = 250$ GeV (200 GeV) at $\mathcal{L} = 500$ fb $^{-1}$. The signal and background cross-sections are 0.11 fb (0.14 fb) and 16.8 fb (12.79 fb), respectively, for $\sqrt{s} = 250$ GeV (200 GeV). Here, the signal cross-section for the 95.5 GeV scalar is obtained by rescaling the one of a hypothetical 95.5 GeV SM Higgs-boson by $\kappa_2^2 = 0.1$.

ear stack of layers, beginning with an input layer of 13 features (kinematic observables) such as the recoil mass, the energies of the b -tagged jets and muons, etc. (see discussion in Appendix A for the list of all the features), reflecting the dimension of input data. The architecture includes six hidden layers with 128, 64, 48, 32, 24, 16 and 8 neurons. Each layer uses the Rectified Linear Unit (ReLU [95]) activation function

$$f(x) \equiv \max(0, x) = \begin{cases} 0 & \text{if } x < 0 \\ x & \text{if } x \geq 0 \end{cases}, \quad (2)$$

where x is the input variable.⁴ It initializes weights for the layers using the HeUniform initializer [96], which draws them from a uniform distribution within the range $[-\sqrt{6/n_i}, \sqrt{6/n_i}]$ based on the number of input neurons n_i connected to the neuron for which weight is initialized. Each layer is followed by a batch normalization to stabilize training and accelerate convergence.⁵ The model concludes with an output layer containing a single neuron and a sigmoid activation function [97]

$$\sigma(x) = \frac{1}{1 + e^{-x}}, \quad \text{with } 0 < \sigma(x) < 1. \quad (3)$$

Here, x is the input variable for the output layer which is the weighted sum of outputs from the previous layer. The weight in the output layer is initialized using the GlorotUniform initializer [98]. The model is compiled with an Adam optimizer [99] with a learning rate of 0.0001. During compilation, the model uses binary cross-entropy [100] with the loss function defined as

$$-f(y_{\text{true}}, y_{\text{pred}}) = y_{\text{true}} \log(y_{\text{pred}}) + (1 - y_{\text{true}}) \log(1 - y_{\text{pred}}), \quad (4)$$

where y_{pred} is the probability that the DNN assigns to an event being signal or background, and y_{true} is the actual class label (1 for signal, 0 for background).

⁴Note that in our analysis, input variables have different scales and units. While we do not normalize input features before training, we employ batch normalization to normalize the mini-batches dynamically during training. This takes into account differences in scale.

⁵Batch normalization stabilizes and accelerates neural network training by standardizing layer inputs, reducing internal covariate shifts, and minimizing variation in input distributions, leading to faster convergence, higher learning rates, and less risk of vanishing or exploding gradients.

With this ML model, we can improve the exploitation of the data to achieve better discrimination between signal and background events, i.e. improve the event classification. For this purpose, the event samples remaining after the optimization cuts are split, with 70% of the events allocated for training the DNN and the remaining 30% reserved for testing its performance. Training is conducted with a batch size of 250 events from shuffled samples of signal and background at both $\sqrt{s} = 250$ GeV and $\sqrt{s} = 200$ GeV. Although the network has a relatively small architecture, it is necessary to check whether it over-fits the training sample by looking at the DNN response, and the probability assigned to each event of being signal or background.

Figure 2a (Figure 2b) shows the normalized number of events to which a specific value of the DNN model response is assigned as well as both signal and background events separately for the training and testing samples for $\sqrt{s} = 250$ GeV (200 GeV). A significant difference is observed between the distributions of the DNN output obtained for the signal and background events. The DNN response demonstrates the classification accuracy of 89.1 (92.3)% for $\sqrt{s} = 250$ GeV (200 GeV) in training. The Receiver Operating Characteristic (ROC) curves provided in Figure 2c and Figure 2d show signal and background efficiencies, i.e. the fraction of signal and background events correctly classified, respectively. The Area Under Curve (AUC) scores for $\sqrt{s} = 250$ GeV (200 GeV), representing the DNN's ability to separate signal and background events across the dataset, are found to be 95.2 (97.4)% and 95 (97.2)% for training and testing samples, respectively. This consistency between training and testing AUC scores suggests that the model generalizes well, capturing signal and background patterns without over-fitting.

2.2. Signal Significance

The signal significance in this study is determined by the following formula

$$S(\delta_{\text{sys}}) = \frac{\mathcal{N}_S}{\sqrt{\mathcal{N}_B + (\delta_{\text{sys}} \cdot \mathcal{N}_B)^2}}. \quad (5)$$

Here, \mathcal{N}_S and \mathcal{N}_B represent the number of signal and background events, respectively, at a given luminosity \mathcal{L} . The term δ_{sys} accounts for systematic uncertainties in the measurement. The number of signal events is defined as $\mathcal{N}_S = \sigma_S \times \mathcal{L}$, where σ_S

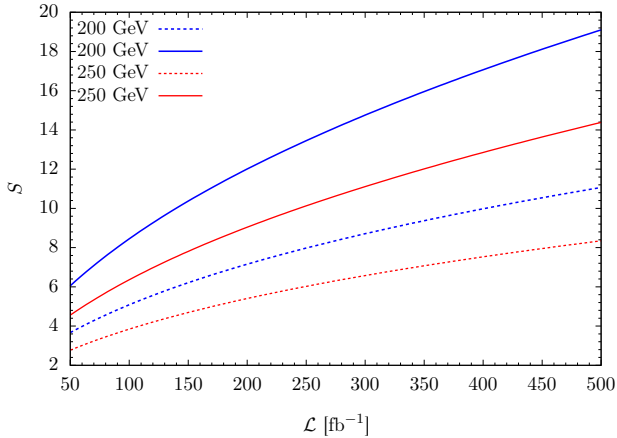


Figure 3: The significance as a function of luminosity for $m_S = 95.5$ GeV and $\sqrt{s} = 250$ GeV (200 GeV) is shown in red (blue). We consider the number of events in the recoil mass window of 93.5 GeV – 97.5 GeV before (after) the DNN has been applied as a dashed (solid) line. A cut of 0.965 (0.959) is applied on DNN response for $\sqrt{s} = 250$ GeV (200 GeV).

represents the cross-section of the BSM signal. Similarly, the number of background events is given by $N_B = \sigma_B \times \mathcal{L}$, where σ_B denotes the cross-section of the SM background.

In Figure 3, we show $S(\delta_{\text{sys}} = 2\%)$ both before and after DNN classification (with recoil mass requirements), as discussed in subsection 2.1, for $\sqrt{s} = 250$ GeV (200 GeV). The analysis is conducted within the range of $93.5 \text{ GeV} \leq M_{\text{recoil}} \leq 97.5 \text{ GeV}$. Comparatively, significance is enhanced after DNN classification. As shown in Table 1 for $\mathcal{L} = 500 \text{ fb}^{-1}$, a significance of approximately 8σ (11σ) can be achieved at a centre-of-mass energy of 200 GeV (250 GeV) before applying the DNN. After applying the DNN, the significance increased to 14σ (19σ).

3. Discovery prospects

We can now consider the discovery prospects for the scalar $m_S \approx 95$ GeV at future e^+e^- colliders. This can be done in a model-independent way by considering its branching ratio to $b\bar{b}$ as well as its coupling to Z-boson (κ_Z). In Figure 4 we present the regions in the κ_Z - $\text{Br}(S \rightarrow b\bar{b})$ plane for $\sqrt{s} = 250$ GeV, $\mathcal{L} = 0.1 \text{ ab}^{-1}$ and 5 ab^{-1} where a discovery is possible. Additionally, we show the preferred region from the analogous LEP measurement and the exclusion from $h \rightarrow \gamma\gamma$ in case S is SM-like, i.e. an $SU(2)_L$ singlet which obtains its couplings from mixing with the SM Higgs. Importantly, one can see that a discovery is possible within the whole 95% confidence-level region preferred by the LEP excess. Note that the sensitivity can be further improved by including additional channels such as $S \rightarrow \tau\tau$ and $Z \rightarrow e^+e^-$.

4. Conclusions and Prospects

In this article, we explore the potential for the production of an additional scalar particle S within the mass range of $m_S = 95 \text{ GeV} - 96 \text{ GeV}$ in an e^+e^- collider environment. Specifically, our investigation focuses on the Circular Electron-Positron

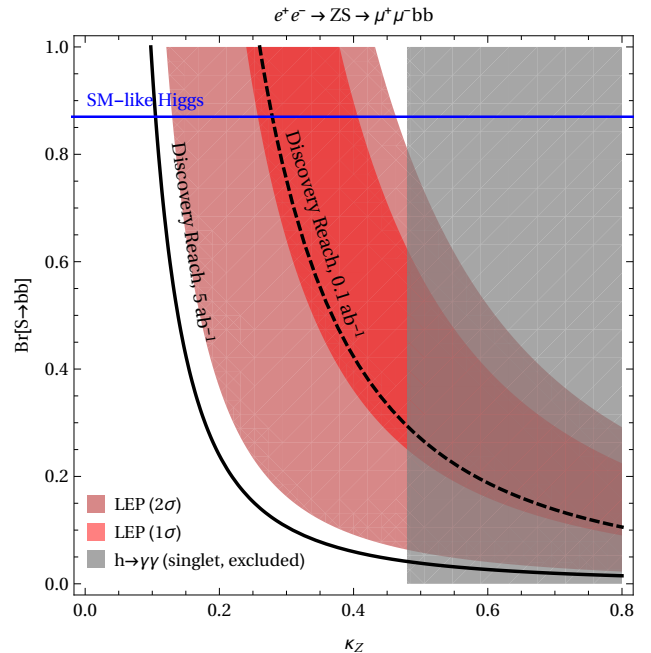


Figure 4: Discovery region for a 95 GeV scalar in the κ_Z - $\text{Br}(S \rightarrow b\bar{b})$ plane for an integrated luminosity of $\mathcal{L} = 5 \text{ ab}^{-1}$ at $\sqrt{s} = 250$ GeV. The green region is currently preferred by the LEP measurement of Higgs-strahlung. The black line indicates the $\text{Br}(S \rightarrow b\bar{b})$ for a SM-like Higgs, and the gray region is excluded by the di-photon signal strength of the SM Higgs assuming that S is an $SU(2)_L$ singlet.

Collider (CEPC) with center-of-mass energies of $\sqrt{s} = 200$ GeV and 250 GeV with an integrated luminosity of $\mathcal{L} = 500 \text{ fb}^{-1}$. The choice of utilizing ML techniques, particularly DNNs, is motivated by their proven accuracy in event classification, as detailed in Ref. [101].

We first demonstrated the advantage of employing DNNs by examining the reconstruction of the scalar mass, m_S , using the recoil mass method within the aforementioned range, as depicted in Figure 1. The effectiveness of DNNs in enhancing signal significance versus luminosity is evident in Figure 3, where a substantial improvement in the signal significance is observed after implementing the DNN. To be more specific, using the DNN our analysis demonstrates that a significance of $\approx 8\sigma$ ($\approx 11\sigma$) for a new scalar with a mass of 95.5 GeV and $\kappa_Z^2 = 0.1$ can be achieved at a c.o.m. energy of GeV (250 GeV) for $\mathcal{L} = 500 \text{ fb}^{-1}$ which corresponds to an increase of 75% (73%). This highlights the critical role of ML techniques in enhancing the sensitivity of collider measurements.

Electron-positron Higgs factories offer a unique capability to tag the $e^+e^- \rightarrow ZS$ signal using the recoil mass method, independent of the Higgs boson decay models. Taking the CEPC as an example, which is expected to deliver 5 ab^{-1} at a c.o.m. energy of 240 GeV – 250 GeV over 10 years of data taking [87, 92], it could identify the recoil mass signal of S within approximately 100 days to confirm a 5σ discovery. However, as analyzed in this article, applying an ML technique reduces the time required to achieve this discovery potential to about 34 days. Note that in this analysis, we considered a tagging efficiency of 80% for b -tagged jets, based on the proposed CEPC detector design.

However, this efficiency could be improved to as high as 92%, as studied in Ref. [102], which would further enhance the significance and discovery potential of the 95 GeV signal.

Appendix A. Input features for event classification in DNN

For the event classification via the DNN, we use 16 observables, including angular observables as well as quantities which have dimensions of mass. Concerning the former, we use azimuthal angle of the b -tagged jets ($\phi_{b1,b2}$) and muons (ϕ_{μ^+, μ^-}), polar angle of the b -tagged jets ($\theta_{b1,b2}$) and the muons (θ_{μ^+, μ^-}). For the observables with mass dimensions, we include the energies of b -tagged jets ($E_{b1,b2}$) and muons (E_{μ^+, μ^-}), the invariant mass of the b -tagged jets ($M_{b\bar{b}}$), the recoil mass of the muons (M_{recoil}), and the visible mass (M_{vis}), which is the invariant mass of the four final-state particles: the two b -jets and two muons. Figure A.5a and Figure A.5b illustrate the correlations between these 16 observables for both signal and background events at a c.o.m. energy of $\sqrt{s} = 250$ GeV. Due to the high correlation observed, we exclude E_{μ^-} , $M_{b\bar{b}}$ and M_{vis} from the analysis and only use the remaining 13 observables as input features for the event classification. Similarly, Figure A.6a and Figure A.6b show the correlation between 16 observables for a centre-of-mass energy of $\sqrt{s} = 200$ GeV. In addition to the correlation found in the case of 250 GeV, we notice a significant correlation between θ_{μ^+} and θ_{μ^-} for both signal and background. However, the use of this observable as an input feature for the DNN does not affect the classification performance, we use the same 13 features as for analysis at $\sqrt{s} = 200$ GeV.

Appendix B. Exploring 95 GeV within the 2HDMS

In connection with the main texts of this article and studies related to explaining the multi-lepton anomalies within the context of a two-Higgs doublet model with an additional singlet scalar S , referred to as the 2HDM+S model [54, 66–70], we investigate the parameter space of the model to identify regions where a scalar of mass $m_S = 95$ GeV can be effectively probed. Here, we will provide a brief exploration of the model parameters and examine the region in which the lightest scalar has a mass around $m_S \approx 95$ GeV and can account for the 95 GeV excesses.

Within the 2HDM+S framework, the potential is given by:

$$\begin{aligned}
V(\Phi_1, \Phi_2, \Phi_S) = & m_{11}^2 |\Phi_1|^2 + m_{22}^2 |\Phi_2|^2 - m_{12}^2 (\Phi_1^\dagger \Phi_2 + \text{h.c.}) \\
& + \frac{\lambda_1}{2} (\Phi_1^\dagger \Phi_1) + \frac{\lambda_2}{2} (\Phi_2^\dagger \Phi_2) + \lambda_3 (\Phi_1^\dagger \Phi_1) (\Phi_2^\dagger \Phi_2) \\
& + \lambda_4 (\Phi_1^\dagger \Phi_2) (\Phi_2^\dagger \Phi_1) + \frac{\lambda_5}{2} [(\Phi_1^\dagger \Phi_2)^2 + \text{h.c.}] \\
& + \frac{1}{2} m_S^2 \Phi_S^2 + \frac{\lambda_6}{8} \Phi_S^4 + \frac{\lambda_7}{2} (\Phi_1^\dagger \Phi_1) \Phi_S^2 + \frac{\lambda_8}{2} (\Phi_2^\dagger \Phi_2) \Phi_S^2.
\end{aligned} \tag{B.1}$$

Here, the fields Φ_1 and Φ_2 represent $SU(2)_L$ Higgs doublets, while the singlet field is represented by Φ_S . After the electroweak symmetry breaking and employing the complete appropriate formalism discussed in Refs. [66, 103], the scalar

spectrum is populated with three CP-even (h_1, h_2, h_3), one CP-odd (A), and one charged (H^\pm) Higgs bosons. Considering the conventions explained in [103, 104], we explore the following set of input parameters, particularly for Type-II 2HDM+S:

$$\left. \begin{aligned}
-\frac{\pi}{2} \leq \alpha_{1,2,3} \leq \frac{\pi}{2}, \quad 1.5 \leq \tan \beta \leq 10, \\
\nu = 256 \text{ GeV}, \quad 40 \text{ GeV} \leq \nu_S \leq 2000 \text{ GeV}, \\
94 \text{ GeV} \lesssim m_{h_1} \lesssim 96 \text{ GeV}, \quad m_{h_2} = 125 \text{ GeV}, \\
500 \text{ GeV} \leq m_{h_3}, m_A \leq 1000 \text{ GeV}, \\
650 \text{ GeV} \leq m_{H^\pm} \leq 1500 \text{ GeV}, \\
400 \text{ GeV} \leq m_{12}^2 \leq 10^6 \text{ GeV}.
\end{aligned} \right\} \tag{B.2}$$

We utilize the ScannerS tool [103], leveraging its feature to assess the parameters space of the model at 95% C.L. under possible theoretical and experimental constraints. The theoretical constraints that ScannerS uses is perturbative unitarity, vacuum stability, and boundedness from below, and the experimental constraints are the electroweak precision observables, flavour physics and Higgs constraints (HiggsSignals and HiggsBounds [105]). We conduct a χ^2 -analysis to quantify the agreement between theoretically predicted signal rates and the experimentally observed values. The χ_{XX}^2 is defined as:

$$\chi_{XX}^2 = \frac{(\mu_{XX} - \mu_{XX}^{\text{exp}})^2}{(\Delta \mu_{XX}^{\text{exp}})^2}, \tag{B.3}$$

where the signal strengths μ_{XX} are derived as a fraction of the product of cross-sections and branching ratios of the BSM over the SM at the same mass:

$$\mu_{XX} = \frac{\sigma^{\text{BSM}}(gg \rightarrow h_i) \times \text{BR}^{\text{BSM}}(h_i \rightarrow XX)}{\sigma^{\text{SM}}(gg \rightarrow H(m_{h_i})) \times \text{BR}^{\text{SM}}(H(m_{h_i}) \rightarrow XX)}, \tag{B.4}$$

and $i = h_1, h_2, h_3, A, H^\pm$. Corresponding to an excess of scalar resonance with $m_{h_1} \approx 95$ GeV in $X = \gamma, b$ and τ channels, the signal strengths are reported as [20, 54, 106]:

$$\mu_{\gamma\gamma}^{\text{exp}} \pm \Delta \mu_{\gamma\gamma}^{\text{exp}} = 0.27_{-0.09}^{+0.10}, \tag{B.5}$$

$$\mu_{bb}^{\text{exp}} \pm \Delta \mu_{bb}^{\text{exp}} = 0.117 \pm 0.057, \tag{B.6}$$

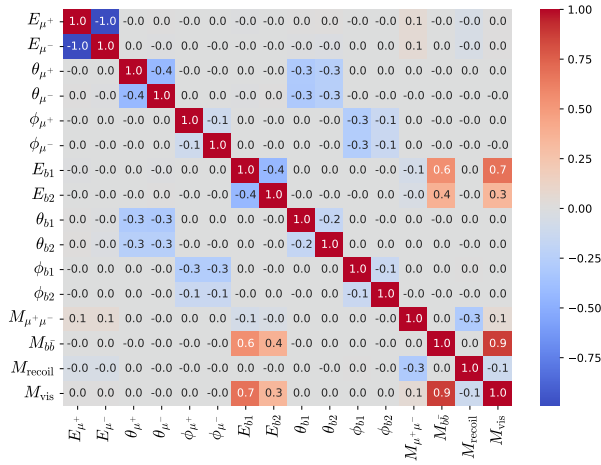
$$\mu_{\tau\tau}^{\text{exp}} \pm \Delta \mu_{\tau\tau}^{\text{exp}} = 0.6 \pm 0.25, \tag{B.7}$$

and for $X = W$ [17]:

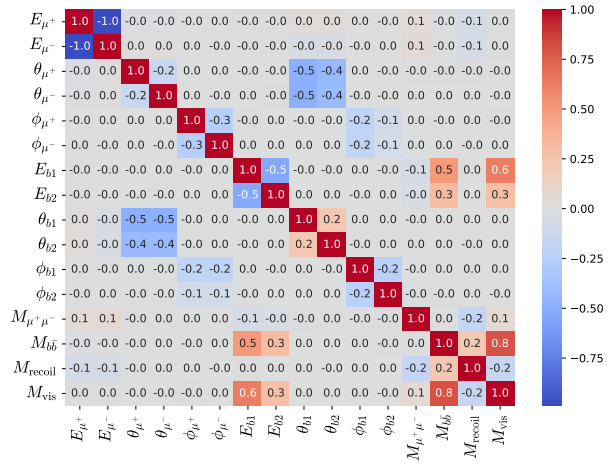
$$\mu_{WW}^{\text{exp}} \pm \Delta \mu_{WW}^{\text{exp}} = 14.6 \pm 6.8. \tag{B.8}$$

The uncertainties $\Delta \mu_{XX}^{\text{exp}}$ from experiments are reported as 1σ variations. In order to evaluate the comprehensive representation of the three excesses, along with an extra excess in the WW channel, we establish the cumulative χ_{95}^2 contribution as follows:

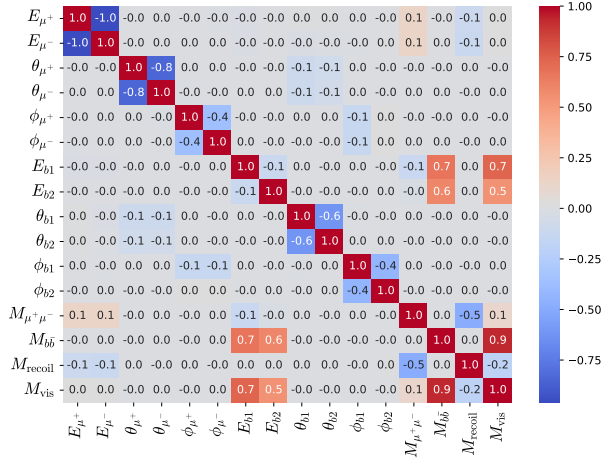
$$\chi_{95}^2 = \chi_{\gamma\gamma}^2 + \chi_{\tau^+\tau^-}^2 + \chi_{bb}^2 + \chi_{WW}^2, \tag{B.9}$$



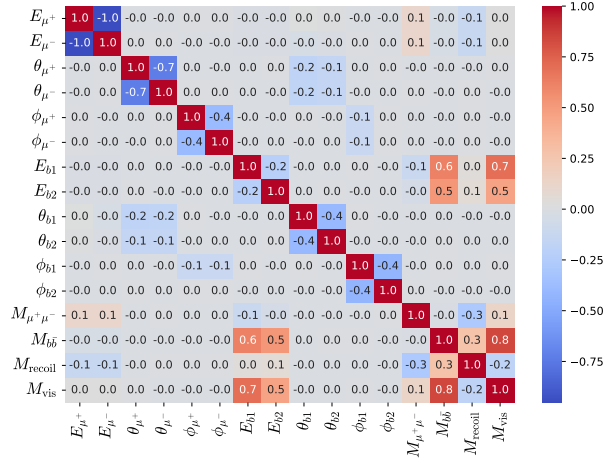
(a)



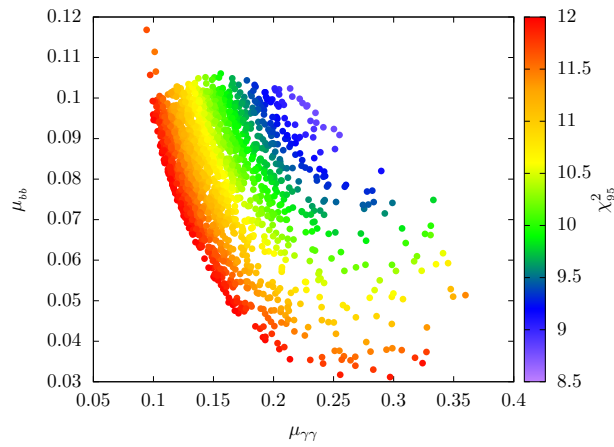
(b)

Figure A.5: Correlation between kinematic observables selected as input features for DNN classification of signal (left) and background (right) at $\sqrt{s} = 250$ GeV.

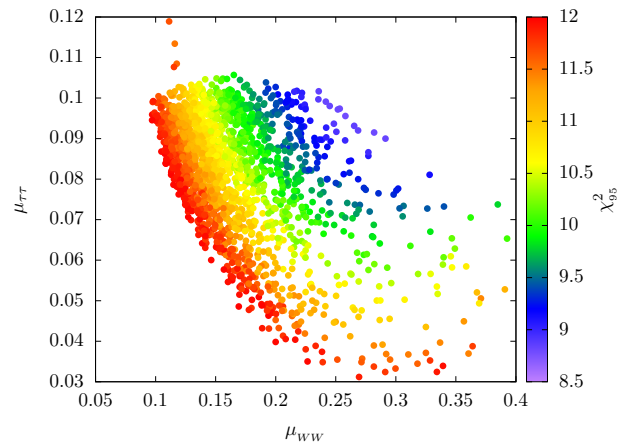
(a)



(b)

Figure A.6: Correlation between kinematic observables selected as input features for DNN classification of signal (left) and background (right) at $\sqrt{s} = 200$ GeV.

(a)



(b)

Figure B.7: The signal strengths of the different final states for the 95 GeV scalar are depicted as a function of the total χ_{95}^2 . Each point satisfies the condition $\chi_{95}^2 < 12$. (a) The signal strengths of $\gamma\gamma$ and $b\bar{b}$ are shown. (b) The signal strengths of the WW and $\tau\tau$ signal strength. Each point satisfies the condition $\chi_{95}^2 < 12$.

where the results for the four channels in which the excesses observed are treated as independent measurements. Thus, we can add the four individual χ^2 contributions.

In the subsequent quantitative examination, we consider parameter points as suitable representations of the excess phenomena if they can effectively explain the collective impact of the four separate excesses with a confidence level of at least 1σ . In the case of four measurements being considered independently, this criterion corresponds to the condition that $\chi_{95}^2 \leq 12$. The results of these scans are shown in Figure B.7.

The scanned parameter space observed in Figure B.7 can further be utilized to study di-boson signatures at the LHC following $gg \rightarrow h_3 \rightarrow h_1 h_2$ with mass constraints studied in [66]. This aligns with the prospects discussed for the observed multi-lepton anomalies.

References

- [1] Peter W. Higgs. Broken symmetries, massless particles and gauge fields. *Phys. Lett.*, 12:132–133, 1964.
- [2] F. Englert and R. Brout. Broken Symmetry and the Mass of Gauge Vector Mesons. *Phys. Rev. Lett.*, 13:321–323, 1964.
- [3] Peter W. Higgs. Broken Symmetries and the Masses of Gauge Bosons. *Phys. Rev. Lett.*, 13:508–509, 1964.
- [4] G. S. Guralnik, C. R. Hagen, and T. W. B. Kibble. Global Conservation Laws and Massless Particles. *Phys. Rev. Lett.*, 13:585–587, 1964.
- [5] Georges Aad et al. Observation of a new particle in the search for the Standard Model Higgs boson with the ATLAS detector at the LHC. *Phys. Lett. B*, 716:1–29, 2012.
- [6] Serguei Chatrchyan et al. Observation of a New Boson at a Mass of 125 GeV with the CMS Experiment at the LHC. *Phys. Lett. B*, 716:30–61, 2012.
- [7] Steven Weinberg. A Model of Leptons. *Phys. Rev. Lett.*, 19:1264–1266, 1967.
- [8] Abdus Salam. Weak and Electromagnetic Interactions. *Conf. Proc. C*, 680519:367–377, 1968.
- [9] S. L. Glashow, J. Iliopoulos, and L. Maiani. Weak Interactions with Lepton-Hadron Symmetry. *Phys. Rev. D*, 2:1285–1292, 1970.
- [10] R. Barate et al. Search for the standard model Higgs boson at LEP. *Phys. Lett. B*, 565:61–75, 2003.
- [11] Patrick Janot. The infamous 95 GeV $b\bar{b}$ excess at LEP: two b or not two b? *JHEP*, 10:223, 2024.
- [12] Albert M Sirunyan et al. Search for a standard model-like Higgs boson in the mass range between 70 and 110 GeV in the diphoton final state in proton-proton collisions at $\sqrt{s} = 8$ and 13 TeV. *Phys. Lett. B*, 793:320–347, 2019.
- [13] Search for a standard model-like Higgs boson in the mass range between 70 and 110 GeV in the diphoton final state in proton-proton collisions at $\sqrt{s} = 13$ TeV. 2023. CMS-PAS-HIG-20-002.
- [14] Search for diphoton resonances in the 66 to 110 GeV mass range using 140 fb⁻¹ of 13 TeV pp collisions collected with the ATLAS detector. 2023. ATLAS-CONF-2023-035.
- [15] Armen Tumasyan et al. Searches for additional Higgs bosons and for vector leptiquarks in $\tau\tau$ final states in proton-proton collisions at $\sqrt{s} = 13$ TeV. *JHEP*, 07:073, 2023.
- [16] Georges Aad et al. Measurements of Higgs boson production cross-sections in the $H \rightarrow \tau^+ \tau^-$ decay channel in pp collisions at $\sqrt{s} = 13$ TeV with the ATLAS detector. *JHEP*, 08:175, 2022.
- [17] Guglielmo Coloretti, Andreas Crivellin, Srimoy Bhattacharya, and Bruce Mellado. Searching for low-mass resonances decaying into W bosons. *Phys. Rev. D*, 108(3):035026, 2023.
- [18] Armen Tumasyan et al. Measurements of the Higgs boson production cross section and couplings in the W boson pair decay channel in proton-proton collisions at $\sqrt{s} = 13$ TeV. *Eur. Phys. J. C*, 83(7):667, 2023.
- [19] Georges Aad et al. Measurements of Higgs boson production by gluon-gluon fusion and vector-boson fusion using $H \rightarrow WW^* \rightarrow e\nu\mu\nu$ decays in pp collisions at $\sqrt{s} = 13$ TeV with the ATLAS detector. *Phys. Rev. D*, 108:032005, 2023.
- [20] Srimoy Bhattacharya, Guglielmo Coloretti, Andreas Crivellin, Salah-Eddine Dabhi, Yaquan Fang, Mukesh Kumar, and Bruce Mellado. Growing Excesses of New Scalars at the Electroweak Scale. arXiv:2306.17209; PSI-PR-23-21, ZU-TH 31/23, ICPP-70.
- [21] Georges Aad et al. Search for diphoton resonances in the 66 to 110 GeV mass range using pp collisions at $\sqrt{s} = 13$ TeV with the ATLAS detector. 7 2024.
- [22] Aram Hayrapetyan et al. Search for a standard model-like Higgs boson in the mass range between 70 and 110 GeV in the diphoton final state in proton-proton collisions at $\sqrt{s} = 13$ TeV. 5 2024.
- [23] Rachid Benbrik, Mohammed Boukidi, and Stefano Moretti. Superposition of CP-Even and CP-Odd Higgs Resonances: Explaining the 95 GeV Excesses within a Two-Higgs Doublet Model. 5 2024.
- [24] Junjie Cao, Xinglong Jia, and Jingwei Lian. Unified Interpretation of Muon g-2 anomaly, 95 GeV Diphoton, and $b\bar{b}$ Excesses in the General Next-to-Minimal Supersymmetric Standard Model. 2 2024.
- [25] Divya Sachdeva and Soumya Sadhukhan. Discussing 125 GeV and 95 GeV excess in light radion model. *Phys. Rev. D*, 101(5):055045, 2020.
- [26] Brahim Ait-Ouazghour, Mohamed Chabab, and Khalid Goure. Unified Interpretation of 95 GeV Excesses in the Two Higgs Doublet type II Seesaw Model. 10 2024.
- [27] Akshat Khanna, Stefano Moretti, and Agnivo Sarkar. Explaining 95 (or so) GeV Anomalies in the 2-Higgs Doublet Model Type-I. 9 2024.
- [28] J. A. Aguilar-Saavedra, H. B. C amara, F. R. Joaquim, and J. F. Seabra. Confronting the 95 GeV excesses within the U(1)-extended next-to-minimal 2HDM. *Phys. Rev. D*, 108(7):075020, 2023.
- [29] Jan Kalinowski and Wojciech Kotlarski. Interpreting 95 GeV diphoton/ $b\bar{b}$ excesses as a lightest Higgs boson of the MRSSM. *JHEP*, 07:037, 2024.
- [30] Rachid Benbrik, Mohammed Boukidi, Stefano Moretti, and Souad Semlali. Explaining the 96 GeV Di-photon anomaly in a generic 2HDM Type-III. *Phys. Lett. B*, 832:137245, 2022.
- [31] Junjie Cao, Xiaofei Guo, Yangle He, Peiwen Wu, and Yang Zhang. Diphoton signal of the light Higgs boson in natural NMSSM. *Phys. Rev. D*, 95(11):116001, 2017.
- [32] Andreas Crivellin, Julian Heeck, and Dario M uller. Large $h \rightarrow bs$ in generic two-Higgs-doublet models. *Phys. Rev. D*, 97(3):035008, 2018.
- [33] Ulrich Haisch and Augustinas Malinauskas. Let there be light from a second light Higgs doublet. *JHEP*, 03:135, 2018.
- [34] Patrick J. Fox and Neal Weiner. Light Signals from a Lighter Higgs. *JHEP*, 08:025, 2018.
- [35] Da Liu, Jia Liu, Carlos E. M. Wagner, and Xiao-Ping Wang. A Light Higgs at the LHC and the B-Anomalies. *JHEP*, 06:150, 2018.
- [36] Kun Wang, Fei Wang, Jingya Zhu, and Quanlin Jie. The semi-constrained NMSSM in light of muon g-2, LHC, and dark matter constraints. *Chin. Phys. C*, 42(10):103109–103109, 2018.
- [37] Lijia Liu, Haoxue Qiao, Kun Wang, and Jingya Zhu. A Light Scalar in the Minimal Dilaton Model in Light of LHC Constraints. *Chin. Phys. C*, 43(2):023104, 2019.
- [38] T. Biek otter, M. Chakraborti, and S. Heinemeyer. A 96 GeV Higgs boson in the N2HDM. *Eur. Phys. J. C*, 80(1):2, 2020.
- [39] James M. Cline and Takashi Toma. Pseudo-Goldstone dark matter confronts cosmic ray and collider anomalies. *Phys. Rev. D*, 100(3):035023, 2019.
- [40] Kiwoon Choi, Sang Hui Im, Kwang Sik Jeong, and Chan Beom Park. Light Higgs bosons in the general NMSSM. *Eur. Phys. J. C*, 79(11):956, 2019.
- [41] Anirban Kundu, Suvam Maharana, and Poulami Mondal. A 96 GeV scalar tagged to dark matter models. *Nucl. Phys. B*, 955:115057, 2020.
- [42] Junjie Cao, Xinglong Jia, Yuanfang Yue, Haijing Zhou, and Pengxuan Zhu. 96 GeV diphoton excess in seesaw extensions of the natural NMSSM. *Phys. Rev. D*, 101(5):055008, 2020.
- [43] T. Biek otter, M. Chakraborti, and S. Heinemeyer. The ‘‘96 GeV excess’’ at the LHC. *Int. J. Mod. Phys. A*, 36(22):2142018, 2021.
- [44] Ahmed Ali Abdelalim, Biswaranjan Das, Shaaban Khalil, and Stefano Moretti. Di-photon decay of a light Higgs state in the BLSSM. *Nucl. Phys. B*, 985:116013, 2022.
- [45] S. Heinemeyer, C. Li, F. Lika, G. Moortgat-Pick, and S. Paasch. Phenomenology of a 96 GeV Higgs boson in the 2HDM with an additional

- singlet. *Phys. Rev. D*, 106(7):075003, 2022.
- [46] Thomas Biekötter, Sven Heinemeyer, and Georg Weiglein. Mounting evidence for a 95 GeV Higgs boson. *JHEP*, 08:201, 2022.
- [47] Syuhei Iguro, Teppei Kitahara, and Yuji Omura. Scrutinizing the 95–100 GeV di-tau excess in the top associated process. *Eur. Phys. J. C*, 82(11):1053, 2022.
- [48] Weichao Li, Haoxue Qiao, and Jingya Zhu. Light Higgs boson in the NMSSM confronted with the CMS di-photon and di-tau excesses*. *Chin. Phys. C*, 47(12):123102, 2023.
- [49] Syuhei Iguro, Teppei Kitahara, Yuji Omura, and Hantian Zhang. Chasing the two-Higgs doublet model in the di-Higgs boson production. *Phys. Rev. D*, 107(7):075017, 2023.
- [50] Thomas Biekötter, Sven Heinemeyer, and Georg Weiglein. The CMS di-photon excess at 95 GeV in view of the LHC Run 2 results. *Phys. Lett. B*, 846:138217, 2023.
- [51] Cesar Bonilla, A. E. Carcamo Hernandez, Sergey Kovalenko, H. Lee, R. Pasechnik, and Ivan Schmidt. Fermion mass hierarchy in an extended left-right symmetric model. *JHEP*, 12:075, 2023.
- [52] Duarte Azevedo, Thomas Biekötter, and P. M. Ferreira. 2HDM interpretations of the CMS diphoton excess at 95 GeV. *JHEP*, 11:017, 2023.
- [53] Sumit Banik, Andreas Crivellin, Syuhei Iguro, and Teppei Kitahara. Asymmetric di-Higgs signals of the next-to-minimal 2HDM with a $U(1)$ symmetry. *Phys. Rev. D*, 108(7):075011, 2023.
- [54] Thomas Biekötter, Sven Heinemeyer, and Georg Weiglein. 95.4 GeV diphoton excess at ATLAS and CMS. *Phys. Rev. D*, 109(3):035005, 2024.
- [55] Pablo Escribano, Víctor Martín Lozano, and Avelino Vicente. Scotogenic explanation for the 95 GeV excesses. *Phys. Rev. D*, 108(11):115001, 2023.
- [56] Alexander Belyaev, Rachid Benbrik, Mohammed Boukidi, Manimala Chakraborti, Stefano Moretti, and Souad Semlali. Explanation of the Hints for a 95 GeV Higgs Boson within a 2-Higgs Doublet Model. 6 2023.
- [57] Sumit Banik, Guglielmo Coloretti, Andreas Crivellin, and Bruce Mellado. Uncovering New Higgses in the LHC Analyses of Differential $t\bar{t}$ Cross Sections. 8 2023.
- [58] Guglielmo Coloretti, Andreas Crivellin, and Bruce Mellado. Combined explanation of LHC multilepton, diphoton, and top-quark excesses. *Phys. Rev. D*, 110(7):073001, 2024.
- [59] M. Maniatis and O. Nachtmann. CMS results for the $\gamma\gamma$ production at the LHC: do they give a hint for a Higgs boson of the maximally CP symmetric two-Higgs-doublet model? 9 2023.
- [60] Ulrich Ellwanger and Cyril Hugonie. Additional Higgs Bosons near 95 and 650 GeV in the NMSSM. *Eur. Phys. J. C*, 83(12):1138, 2023.
- [61] Jon Butterworth, Hridoy Debnath, Pavel Fileviez Perez, and Francis Mitchell. Custodial Symmetry Breaking and Higgs Signatures at the LHC. 9 2023.
- [62] Amine Ahriche, Mohamed Lamine Bellilet, Mohammed Omer Khojali, Mukesh Kumar, and Anza-Tshildzi Mulaudzi. Scale invariant scotogenic model: CDF-II W-boson mass and the 95 GeV excesses. *Phys. Rev. D*, 110(1):015025, 2024.
- [63] Junjie Cao, Xinglong Jia, Jingwei Lian, and Lei Meng. 95 GeV Diphoton and $b\bar{b}$ Excesses in the General Next-to-Minimal Supersymmetric Standard Model. 10 2023.
- [64] P. S. Bhupal Dev, Rabindra N. Mohapatra, and Yongchao Zhang. Explanation of the 95 GeV $\gamma\gamma$ and $b\bar{b}$ excesses in the minimal left-right symmetric model. *Phys. Lett. B*, 849:138481, 2024.
- [65] Weichao Li, Haoxue Qiao, Kun Wang, and Jingya Zhu. Light dark matter confronted with the 95 GeV diphoton excess. 12 2023.
- [66] Stefan von Buddenbrock, Nabarun Chakraborty, Alan S. Cornell, Deepak Kar, Mukesh Kumar, Tanumoy Mandal, Bruce Mellado, Biswarup Mukhopadhyaya, Robert G. Reed, and Xifeng Ruan. Phenomenological signatures of additional scalar bosons at the LHC. *Eur. Phys. J. C*, 76(10):580, 2016.
- [67] Stefan von Buddenbrock, Alan S. Cornell, Abdualazem Fadol, Mukesh Kumar, Bruce Mellado, and Xifeng Ruan. Multi-lepton signatures of additional scalar bosons beyond the Standard Model at the LHC. *J. Phys. G*, 45(11):115003, 2018.
- [68] Stefan Buddenbrock, Alan S. Cornell, Yaquan Fang, Abdualazem Fadol Mohammed, Mukesh Kumar, Bruce Mellado, and Kehinde G. Tomiwa. The emergence of multi-lepton anomalies at the LHC and their compatibility with new physics at the EW scale. *JHEP*, 10:157, 2019.
- [69] Yesenia Hernandez, Mukesh Kumar, Alan S. Cornell, Salah-Eddine Dahbi, Yaquan Fang, Benjamin Lieberman, Bruce Mellado, Kgomotso Monnakgotla, Xifeng Ruan, and Shuting Xin. The anomalous production of multi-lepton and its impact on the measurement of Wh production at the LHC. *Eur. Phys. J. C*, 81(4):365, 2021.
- [70] Stefan von Buddenbrock, Richard Ruiz, and Bruce Mellado. Anatomy of inclusive $t\bar{t}W$ production at hadron colliders. *Phys. Lett. B*, 811:135964, 2020.
- [71] Oliver Fischer et al. Unveiling hidden physics at the LHC. *Eur. Phys. J. C*, 82(8):665, 2022.
- [72] Andreas Crivellin and Bruce Mellado. Anomalies in Particle Physics. 9 2023.
- [73] Albert M Sirunyan et al. Search for heavy Higgs bosons decaying to a top quark pair in proton-proton collisions at $\sqrt{s} = 13$ TeV. *JHEP*, 04:171, 2020. [Erratum: *JHEP* 03, 187 (2022)].
- [74] Mingyi Dong et al. CEPC Conceptual Design Report: Volume 2 - Physics & Detector. 11 2018.
- [75] Fenfen An et al. Precision Higgs physics at the CEPC. *Chin. Phys. C*, 43(4):043002, 2019.
- [76] T. K. Charles et al. The Compact Linear Collider (CLIC) - 2018 Summary Report. 2/2018, 12 2018.
- [77] A. Abada et al. FCC-ee: The Lepton Collider: Future Circular Collider Conceptual Design Report Volume 2. *Eur. Phys. J. ST*, 228(2):261–623, 2019.
- [78] A. Abada et al. FCC Physics Opportunities: Future Circular Collider Conceptual Design Report Volume 1. *Eur. Phys. J. C*, 79(6):474, 2019.
- [79] The International Linear Collider Technical Design Report - Volume 2: Physics. 6 2013.
- [80] The International Linear Collider Technical Design Report - Volume 3.I: Accelerator & in the Technical Design Phase. 6 2013.
- [81] H. Abramowicz et al. Physics at the CLIC e^+e^- Linear Collider – Input to the Snowmass process 2013. In *Snowmass 2013: Snowmass on the Mississippi*, 7 2013.
- [82] S. Agostinelli et al. GEANT4—a simulation toolkit. *Nucl. Instrum. Meth. A*, 506:250–303, 2003.
- [83] J. Allison et al. Recent developments in Geant4. *Nucl. Instrum. Meth. A*, 835:186–225, 2016.
- [84] Physics and Detectors at CLIC: CLIC Conceptual Design Report. 2 2012.
- [85] P. Lebrun, L. Linssen, A. Lucaci-Timoce, D. Schulte, F. Simon, S. Stapanes, N. Toge, H. Weerts, and J. Wells. The CLIC Programme: Towards a Staged e^+e^- Linear Collider Exploring the Terascale : CLIC Conceptual Design Report. 9 2012.
- [86] Halina Abramowicz et al. The International Linear Collider Technical Design Report - Volume 4: Detectors. 6 2013.
- [87] Zhenxing Chen, Ying Yang, Manqi Ruan, Dayong Wang, Gang Li, Shan Jin, and Yong Ban. Cross Section and Higgs Mass Measurement with Higgsstrahlung at the CEPC. *Chin. Phys. C*, 41(2):023003, 2017.
- [88] Johan Alwall, Michel Herquet, Fabio Maltoni, Olivier Mattelaer, and Tim Stelzer. MadGraph 5 : Going Beyond. *JHEP*, 06:128, 2011.
- [89] Christian Bierlich et al. A comprehensive guide to the physics and usage of PYTHIA 8.3. *SciPost Phys. Codeb.*, 2022:8, 2022.
- [90] J. de Favereau, C. Delaere, P. Demin, A. Giammanco, V. Lemaître, A. Mertens, and M. Selvaggi. DELPHES 3, A modular framework for fast simulation of a generic collider experiment. *JHEP*, 02:057, 2014.
- [91] Cheng Chen, Xin Mo, Michele Selvaggi, Qiang Li, Gang Li, Manqi Ruan, and Xinchou Lou. Fast simulation of the CEPC detector with Delphes. 12 2017.
- [92] Waleed Abdallah et al. CEPC Technical Design Report – Accelerator (v2). 12 2023.
- [93] Matteo Cacciari, Gavin P. Salam, and Gregory Soyez. FastJet User Manual. *Eur. Phys. J. C*, 72:1896, 2012.
- [94] Matteo Cacciari, Gavin P. Salam, and Gregory Soyez. The anti- k_r jet clustering algorithm. *JHEP*, 04:063, 2008.
- [95] Abien Fred Agarap. Deep Learning using Rectified Linear Units (ReLU). 3 2018.
- [96] Kaiming He, Xiangyu Zhang, Shaoqing Ren, and Jian Sun. Delving deep into rectifiers: Surpassing human-level performance on imagenet classification. *Proceedings of the IEEE International Conference on Computer Vision*, 2015.
- [97] Sridhar Narayan. The generalized sigmoid activation function: Competitive supervised learning. *Information sciences*, 99(1-2):69–82, 1997.

- [98] Xavier Glorot and Yoshua Bengio. Understanding the difficulty of training deep feedforward neural networks. In Yee Whye Teh and Mike Titterton, editors, *Proceedings of the Thirteenth International Conference on Artificial Intelligence and Statistics*, volume 9 of *Proceedings of Machine Learning Research*, pages 249–256, Chia Laguna Resort, Sardinia, Italy, 13–15 May 2010. PMLR.
- [99] D Kinga, Jimmy Ba Adam, et al. A method for stochastic optimization. In *International conference on learning representations (ICLR)*, volume 5, page 6. San Diego, California, 2015.
- [100] Christopher M Bishop. *Pattern recognition and machine learning*. 2006.
- [101] Torben Lange, Saswati Nandan, Joosep Pata, Laurits Tani, and Christian Veelken. Particle-flow based tau identification at future e^+e^- colliders. 7 2023.
- [102] Hao Liang, Yongfeng Zhu, Yuexin Wang, Yuzhi Che, Manqi Ruan, Chen Zhou, and Huilin Qu. Jet-origin identification and its application at an electron-positron higgs factory. *Phys. Rev. Lett.*, 132:221802, May 2024.
- [103] Margarete Muhlleitner, Marco O. P. Sampaio, Rui Santos, and Jonas Wittbrodt. The N2HDM under Theoretical and Experimental Scrutiny. *JHEP*, 03:094, 2017.
- [104] Stefan von Buddenbrock, Alan S. Cornell, Elie D. R. Iarilala, Mukesh Kumar, Bruce Mellado, Xifeng Ruan, and Esra Mohammed Shrif. Constraints on a 2HDM with a singlet scalar and implications in the search for heavy bosons at the LHC. *J. Phys. G*, 46(11):115001, 2019.
- [105] Henning Bahl, Thomas Biekötter, Sven Heinemeyer, Cheng Li, Steven Paasch, Georg Weiglein, and Jonas Wittbrodt. HiggsTools: BSM scalar phenomenology with new versions of HiggsBounds and HiggsSignals. *Comput. Phys. Commun.*, 291:108803, 2023.
- [106] G. Abbiendi et al. Decay mode independent searches for new scalar bosons with the OPAL detector at LEP. *Eur. Phys. J. C*, 27:311–329, 2003.